RSC Advances

ROYAL SOCIETY OF CHEMISTRY

PAPER

View Article Online
View Journal | View Issue

Cite this: *RSC Adv.*, 2026, **16**, 700

Comparative DFT analysis of CO_2 cycloaddition with ionic liquids in encapsulated and free states

Annum Ahsan,[a] Ahmed Lakhani [b] and Khurshid Ayub *[a]

The conversion of CO_2 into valuable products offers a promising route for both its mitigation and utilization. Ionic liquids (ILs), particularly in encapsulated forms (ENILs), have shown great potential for CO_2 capture, yet their application in CO_2 conversion remains underexplored. In this study, we present the first density functional theory (DFT) investigation of CO_2 conversion to cyclic carbonate using belt[14]pyridine-encapsulated tetramethylammonium chloride (BP-TMACl) in reaction with propylene oxide. The results reveal that encapsulation significantly reduces the activation barriers compared to unencapsulated TMACl. The energy barrier for propylene oxide ring-opening decreases from 34.95 kcal mol^{-1} to 33.73 kcal mol^{-1}, while the second step—CO_2 insertion and cyclization—shows a more substantial reduction from 18.09 kcal mol^{-1} to 10.00 kcal mol^{-1}. Non-covalent interaction (NCI) and quantum theory of atoms in molecules (QTAIM) analyses indicate that the confinement effect within the capsule stabilizes both reactants and transition states, lowering the energy difference and enhancing reaction feasibility. The overall reaction remains exergonic, with improved thermodynamic favorability for the encapsulated system. These findings demonstrate that encapsulated ILs, such as BP-TMACl, can significantly enhance CO_2 conversion efficiency, offering a more effective and economically viable approach for CO_2 utilization.

Received 26th August 2025
Accepted 14th December 2025

DOI: 10.1039/d5ra06369h

rsc.li/rsc-advances

1 Introduction

In the recent years, due to rapid rise of the global population, energy consumption has been growing significantly. One of the main energy sources in the world is fossil fuel. The global use of fossil fuels has led to serious environmental problems caused by carbon emissions. Carbon dioxide (CO_2) is an important heat trapping (greenhouse) gas, which is released by burning of fossil fuels. In addition to burning of fossil fuel, other anthropogenic activities which are the source of CO_2 emission are deforestation, transportation and industrial activities.[1] It is also produced by natural processes, such as respiration and volcanic eruptions. According to the literature, CO_2 concentration in the atmosphere has dramatically boosted from 340 ppm in 1980 to 422 ppm in 2022 leading to an adverse impact on the environment.[2]

To reduce the emission of CO_2, various processes have been introduced like pre-combustion techniques,[3] post combustion techniques,[4] oxyfuel combustion,[5] and storage of CO_2 after production. Pre-combustion technique involves removal of carbon from the fuel *i.e.*, gas or coal, before combustion process. In this process, the fossil fuels are transformed into synthesis gas, *i.e.*, a mixture of CO + H_2 (syn-gas).[6] The carbon-monoxide portion of syn-gas is converted further to carbon-dioxide. At this stage, mixture of CO_2 and H_2 is obtained. CO_2 is further separated from this mixture resulting into production of H_2-rich fuel which is then used for further combustion. Another technique *i.e.*, post combustion capture, comprises of capturing of CO_2 from flue gas streams after fossil fuels have been burned. With this technology, CO_2 is separated from the flue gas by scrubbing with a chemical solvent such as amine. Oxyfuel combustion is another technology in which pure oxygen environment is used for combustion. In this way, flue stream containing concentrated CO_2 is obtained which is easier to separate. Yet another method is CO_2 capture followed by its storage to tackle global warming. From the last few decades, research is focused on transformation of CO_2 into some useful compounds/chemicals and the technologies related to carbon capturing and utilization (CCU) are the focus of interest of many researchers. In these methods, after CO_2 fixation, it is used as a solvent or as a reactant in order to synthesize other organic chemicals.

Among various CO_2 conversion studies, the production of cyclic carbonates from CO_2 (with the help of epoxides) has received substantial interest.[7] The reason is the thermodynamic feasibility, and potential industrial relevance of this process.[8,9] Moreover, the industrial practices used presently also utilize phosgene for preparation of cyclic carbonates.[7] Comparison of use of phosgene with the use of CO_2 in the process of formation

[a]*Department of Chemistry, COMSATS University, Abbottabad Campus, KPK, 22060, Pakistan. E-mail: khurshid@cuiatd.edu.pk; Tel: +92-992-383591*

[b]*Department of Biomedical and Health Sciences, Calumet College of St. Joseph, Whiting, Indiana, 46394, USA*

of cyclic carbonates shows the environmental improvement in case of CO_2 due to highly toxic and corrosive nature of phosgene.[7] On the other hand, CO_2 is not only non-toxic and non-flammable but abundant and economical as well. Moreover, for the preparation of carbonates, ethylene oxide and propylene oxide have most commonly been employed for cycloaddition of CO_2 and as a result ethylene and propylene carbonates are formed.[8] These reactions have been catalyzed by various reagents like metal–organic frameworks,[9] organocatalysts,[10] and ionic liquids.[11] Among all these catalysts, ionic liquids have been divulged as promising candidates for these reactions. The reason is their negligible vapor pressure, favorable solvent properties, high thermal stability, adjustable affinity for CO_2 capture, and non-flammability.[12] A number of different ionic liquids have been used for conversion of CO_2 to cyclic carbonates. The most commonly used ionic liquids are halide ion containing ionic liquids.[12,13] The halide anion containing ionic liquids work by the attack of halide anion on epoxide opening its ring structure easily.[14–16] However, other types of ionic liquids with the anions other than halide have also been[17–22] used including hydroxyl based,[17] triazine based,[21] benzyl based,[20] and carboxylic based ionic liquids[19] *etc*.

Ionic liquids show numerous applications[23–26] in variety of fields and have been considered as one of the most favorable candidates for capturing and conversion of CO_2. Such diverse applications of ionic liquids are due to their distinctive properties like high stability (both thermal and chemical),[27,28] high tenability,[29–31] low melting point, high catalyzing effect, high dissolution ability and high polarity. Despite such diverse applications, the high viscosity[32,33] resulting in low fluidity is still a hurdle while using ionic liquids in such conversion processes. In order to boost the efficiency of ionic liquids, encapsulation of ionic liquids has been considered. Various materials have been introduced to encapsulate ionic liquids including metal organic frameworks,[34] monolithic polymer structures,[35–40] covalent organic frameworks, inside organic and inorganic shells[41,42] and silica monoliths.

The encapsulated ionic liquids (ENILs) are used as catalysts,[43] in sewage purification,[36] and in gas separation.[44] The performance of ionic liquids is improved with encapsulation. A number of studies have been reported showing that ionic liquids in encapsulated forms show efficient gas separation properties and show improvement in separation ability as compared to same ionic liquids in their un-encapsulated forms.[45] An ionic liquid studied for its CO_2 capturing abilities is 1-butyl-3-methylimidazolium tetrafluoroborate + monoethanolamine ([BMIM][BF_4]-MEA). This blend of IL with amine showed CO_2 absorption capacity of 0.2 mol CO_2 per kg in its encapsulated form while its un-encapsulated form absorbed 0.05 mol of CO_2 per kg of the [BMIM][BF_4]-MEA. The results clearly show that the CO_2 absorption capacity is 4× higher with encapsulated version as compared to un-encapsulated version.[46] Yet another study highlights the improved CO_2 capturing abilities of encapsulated ILs *i.e.*, [BMIM][BF_4], [EMIM][BF_4], and [BMIM][PF_6] show absorption capacity of 7.0, 12.3, and 7.1 mmol CO_2 per min, respectively. While, their encapsulated forms (ILs in polymer shells) show enhanced absorption capacity of 31.2, 33.4, and 13.0 mmol CO_2 per min, respectively.[47]

As better CO_2 capturing ability is shown by ENILs as compared to their un-encapsulated analogues hence we expect CO_2 conversion ability of ILs to be improved after encapsulation as well. However, ENILs have not been utilized for conversion of CO_2 so far. In the current study, we have considered an encapsulated ionic liquid *i.e.*, assembled belt[14]pyridine encapsulated tetramethylammonium chloride (BP-TMACl), for conversion of CO_2 in order to explore the CO_2 conversion ability of ENILs for the first time. The encapsulating body in the selected ENILs is belt pyridine. The belt molecules exhibit fully conjugated π-systems showing exceptional supramolecular properties.[48] With excellent complexation properties, belt molecules act as efficient encapsulating bodies for ILs. Moreover, the cavity provided by the belt pyridine individually can be deepened if these belts are stacked or assembled successfully. Furthermore, the encapsulating body participates in capturing of CO_2 and thus it is expected that it will help in CO_2 conversion as well. Additionally, the encapsulated and un-encapsulated forms of TMACl have been used and CO_2 conversion reaction is performed with both in order to compare the efficiency of encapsulated ILs as compared to their un-encapsulated form.

Furthermore, different ionic liquids with different cation–anion combinations have been utilized for conversion of CO_2 up till now.[49] For example, quaternary ammonium (as cation) based IL, imidazolium based IL, and pyridinium based IL have already been tested for their CO_2 conversion capabilities and the results prove pyridinium based ILs as the better choices.[49] Moreover, Br^- based ILs have been proven to be better catalysts in terms of their CO_2 conversion performance as compared to Cl^- based ILs.[50,51] But, ionic liquids in their encapsulated forms have not been tested yet for their CO_2 conversion ability. The purpose of our study is to explore the CO_2 conversion ability of encapsulated IL which hasn't been tested before.

2 Research methodology

The current study focuses on conversion of CO_2 molecule to cyclic carbonate in the presence of IL in its un-encapsulated (TMACl) and encapsulated (BP-TMACl) forms. A detailed mechanistic study has been carried out examining the reaction between an epoxide *i.e.*, propylene oxide and CO_2 in the presence of TMACl and BP-TMACl separately as catalysts. The conversion of CO_2 has been investigated by using Gaussian 09 software.[52] The geometries have been optimized at B3LYP method within Density Functional Theory (DFT) coupled with 6–31G(d,p) basis set. For the confirmation of true minima in optimization processes and location of transition states, vibrational frequency analysis is performed at the same level of theory. Through frequency analysis, the number of imaginary frequencies show that whether a transition state or a minimum has been located. When the results of frequency analysis show all the positive frequencies, it is confirmation of a true minimum while arousal of only one imaginary frequency validates the location of a transition state. Moreover, through

optimization of reactants, products and transition states, the energy barriers are calculated through eqn (1).

$$E_a = E_T - E_R \quad (1)$$

here, E_a represents the energy barrier, E_T denotes the energy of transition state and energy of reactant is represented by E_R.

The Gibbs free energy change (ΔG) has also been computed for each elementary step of the reaction to assess their thermodynamic feasibility through eqn (2).

$$\Delta G = \Delta H - T\Delta S \quad (2)$$

here, ΔG is the change in Gibb's free energy, while ΔH and ΔS are the thermal and entropic corrections obtained from the frequency calculations at 298.15 K.

Additionally, in order to support the reliability of our optimized structures further, we computed the binding energies ($E_{binding}$) of substrate at ionic liquid through the following formula.

$$E_{binding} = E_{complex} - (E_{catalyst} + E_{substrate}) \quad (3)$$

These values of $E_{binding}$ confirm that the substrates bind favorably to all active centers investigated, validating the structural models used for the mechanistic and electronic analyses.

In order to study the orbital interactions between reactants and ILs (BP-TMACl and TMACl), frontier molecular orbital (FMO) analysis is considered first.[53,54]

Moreover, in the process of conversion of CO_2, non-bonding interactions between ILs (both TMACl and BP-TMACl) and the reactants play main role. Therefore, it is imperative to study the varying types of interactions between the fragments of reactant and transition state species. For this purpose, non-covalent interactions (NCI) analysis is opted. It gives visual illustration of different nonbonding interaction forces between fragments in complexes *i.e.*, repulsive forces, London dispersion forces, and electrostatic interactions. The energy barriers can be justified through the study of non-covalent interactions between the fragments of reactants and transition states *i.e.*, the reacting bodies and TMACl/BP-TMACl. The level of theory selected for NCI analysis is ωB97XD/6-31G(d,p). ωB97XD has been chosen due to its inclusion of long-range corrected exchange and empirical dispersion, which provides a more reliable description of non-covalent interactions than B3LYP. The results of NCI analysis calculated at B3LYP6-31G(d,p) are also provided in Fig. S1.

NCI analysis generates 2-D reduced density gradient (RDG) plots of electron density (ρ) *versus* reduced density gradient[55] where,

$$RDG = \frac{1}{2(3\pi)^{1/3}} \frac{\nabla\rho}{\rho^{3/4}} \quad (4)$$

These plots use a color scale to differentiate various non-covalent interactions *i.e.*, blue color represents hydrogen bonding, green color depicts London dispersion forces and red color shows electrostatic repulsions. Along with 2-D plots, NCI analysis also generates 3-D figures of complexes *via* Multiwfn 3.8 software.[56] The mentioned colors also appear in the figures where they help to locate the non-covalent interactions in complexes and further confirm their presence as well.

Additionally, for further exploration of these non-covalent interactions' nature and strength, quantum theory of atoms in molecules (QTAIM) analysis is considered.[57] In QTAIM, different topological parameters *i.e.*, electron density (ρ), Laplacian of electron density ($\nabla^2\rho$), kinetic energy density (Lagrangian) $G_{(r)}$, potential energy density $V_{(r)}$, and total energy density $H_{(r)}$ are calculated in order to understand nature of interactions through bond critical points (BCPs).[58,59] E_{int} of individual bonds is another parameter which helps in yet further estimation of category and strength of non-covalent interactions. Espinosa approach[60] is used for calculation of E_{int}.

$$E_{int}\ (au) = \tfrac{1}{2}V_{(r)} \quad (5)$$

3 Results and discussion

3.1 Mechanism of CO_2 conversion

The coupling reaction between CO_2 and propylene oxide (PO) to produce propylene carbonate (PC) is known to be nearly impossible to accomplish in a benign environment without a catalyst.[61] In this regard, a catalyst is used during the reaction in order to obtain an energy rich substrate or to activate the molecule of CO_2. The well-known mechanisms[62,63] of this reaction involve the nucleophilic attack of anion of the catalyst on the carbon atom of the PO to produce ring opened PO (an energy-rich substrate) while the other well known mechanism is the attack of anion on carbon atom of CO_2 to activate CO_2 molecule for further reaction (both the reaction mechanisms

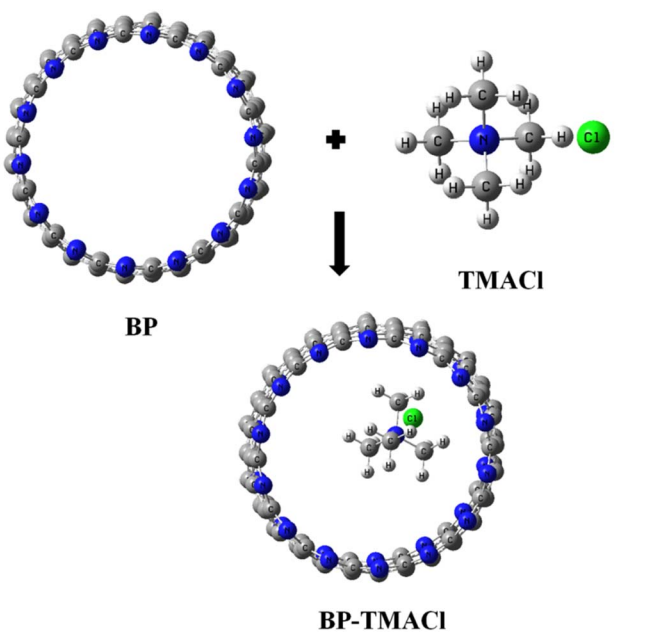

Fig. 1 Encapsulation of TMACl in BP.

are given in Fig. 2). However, the former mechanism is considered as a more competitive and has been testified as the one with lower energy barrier, according to previously reported studies.[62,63] Hence, we have followed the mechanism *i.e.*, the nucleophilic attack of anion of the catalyst on the propylene oxide for ring opening leading to the formation of oxy-anion or a ring-opened substrate.[12] Next step is reaction between the CO_2 and the oxy-anion. These two moieties pass through an intramolecular cyclization reaction to form cyclic carbonate. The catalyst is released at the end as the product forms.[63,64] So, overall it's a three step mechanism involving ring opening, insertion of CO_2 and ring closure.

In the current study, the conversion process involves use of BP-TMACl, an encapsulated ionic liquid as a catalyst. It consists of assembled-belt[14]pyridine with tetramethylammonium chloride encapsulated inside. Fig. 1 shows the encapsulation mechanism for encapsulation of TMACl inside BP. Moreover, an epoxide *i.e.*, propylene oxide (PO), is the other reactant. Propylene oxide (PO) is introduced into the assembled belts near ionic liquid inside the belts' cavity. The reaction starts by the nucleophilic attack of halide ion of the ionic liquid *i.e.*, Cl^-, on the propylene oxide for ring opening. Ring opening leads to the formation of an oxy-anion which further reacts with CO_2 to form cyclic carbonate. The general reaction mechanism of TMACl is given in Fig. 2. The reaction in the figure is given for TMACl without encapsulation. Inside the belt, the reaction occurs through similar mechanism. For the current study, comparison between CO_2 conversion reaction through encapsulated ionic liquid (BP-TMACl) and an un-encapsulated ionic liquid (TMACl) is studied. The reactants, transition states, intermediates and products are represented as R, TS-1/TS-2, Int, and P respectively, for reaction with bare ionic liquid (TMACl). While, for the

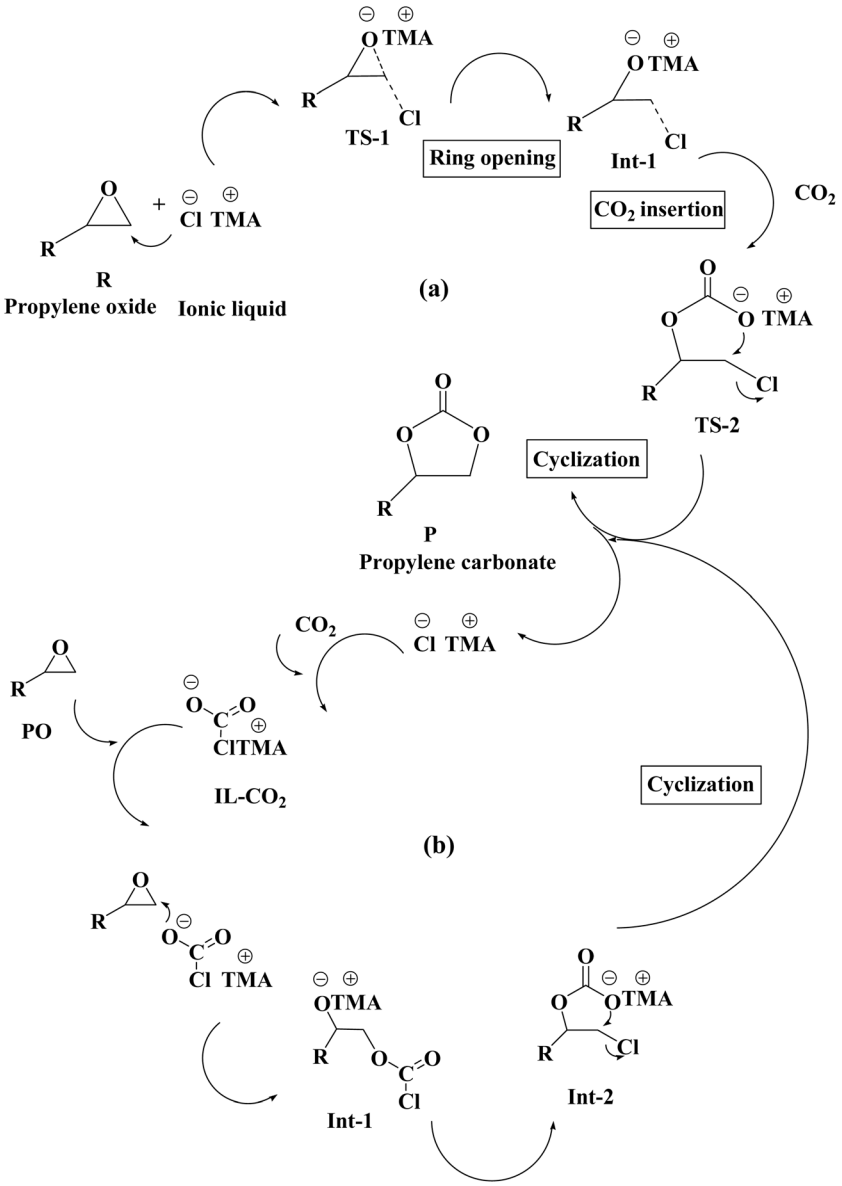

Fig. 2 Schematic illustration of two well-known CO_2 conversion mechanisms: (a) anion-initiated ring opening of propylene oxide (PO); (b) anion-assisted activation of CO_2 *via* nucleophilic attack.

Table 1 Energy barriers (E_a in kcal mol^{-1}), energy of reaction (ΔH in kcal mol^{-1}), Gibb's free energies (ΔG in kcal mol^{-1}), binding energies ($E_{binding}$) for reaction with TMACl and BP-TMACl, energies of HOMO (E_H in eV), energies of LUMO (E_L in eV) and HOMO–LUMO gaps (H–L gaps in eV)

Reacting bodies	Energy barriers	ΔH	ΔG	$E_{binding}$	E_H	E_L	H–L gaps
BP	—	—	—	—	−5.38	−5.12	0.26
R-1	34.95	10.09	12.33	−7.26	−4.49	0.59	3.90
TS-1				—	−4.59	0.07	4.52
P-1				2.84	—	—	—
R-1$_{(E)}$	33.73	11.81	11.08	−20.94	−5.08	−4.82	0.26
TS-1$_{(E)}$				—	−5.08	−4.81	0.27
P-1$_{(E)}$				−9.14	—	—	—
R-2	18.09	11.24	10.59	−18.48	−5.32	0.40	4.92
TS-2				—	−4.99	0.19	4.80
P-2				11.40	—	—	—
R-2$_{(E)}$	10.00	−9.44	−9.84	−20.28	−5.18	−4.91	0.27
TS-2$_{(E)}$				—	−5.23	−4.97	0.26
P-2$_{(E)}$				−27.78	—	—	—

reaction with encapsulated ionic liquid (BP-TMACl), the symbols used are, R$_{(E)}$, TS-1$_{(E)}$/TS-2$_{(E)}$, Int$_{(E)}$, and P$_{(E)}$.

Additionally, in order to support the reliability of optimized structures involved in the reaction, binding energies of substrates at ionic liquid have been calculated. The calculated binding energies ($E_{binding}$) range from −9.14 to −27.78 kcal mol^{-1} for the substrates bound to BP-TMACl while for the substrates bound to TMACl these values range from −18.48 to 11.40 kcal mol^{-1} (given in Table 1). The results show that the $E_{binding}$ are particularly negative for all the substrates bound to BP-TMACl. This shows the more thermodynamically favourable nature of the reaction in the presence of encapsulated ionic liquid.

3.2 Energy barriers

Following the general mechanism (Fig. 2(a)),[64] in the first step, Cl$^-$ of BP-TMACl attacks PO leading to the ring opening of propylene oxide. As discussed earlier, the ring opening resulting in oxy-anion formation proceeds through a transition state. The transition state (TS-1$_{(E)}$) is located at a barrier of 33.73 kcal mol^{-1} for an oxy-anion formation through BP-TMACl while barrier for this step with un-encapsulated TMACl (TS-1) is equal to 34.95 kcal mol^{-1}. The GaussView structures for the reaction mechanisms are given for encapsulated ionic liquid and un-encapsulated ionic liquid in Fig. 4 and 5, respectively. The TS-1 which contains a ring opened oxyanion leads to an intermediate formation (Int$_{(E)}$). The next step involves the reaction between the ring opened oxyanion (an intermediate) and CO_2. The negatively charged oxygen of oxyanion in Int$_{(E)}$ attacks the C-atom of CO_2 and results in formation of cyclic carbonate. This step also proceeds through transition state (TS-2$_{(E)}$) and the energy barrier calculated for locating TS-2$_{(E)}$ in this step is equal to 10.00 kcal mol^{-1} with BP-TMACl. While, energy barrier is equal to 18.09 kcal mol^{-1} (TS-2) with TMACl without encapsulation. While calculating the energy barrier for TS-2/TS-2$_{(E)}$, the difference in energies of TS-2 (TS-2/TS-2$_{(E)}$) and reactant-2 (R-2/R-2$_{(E)}$) is

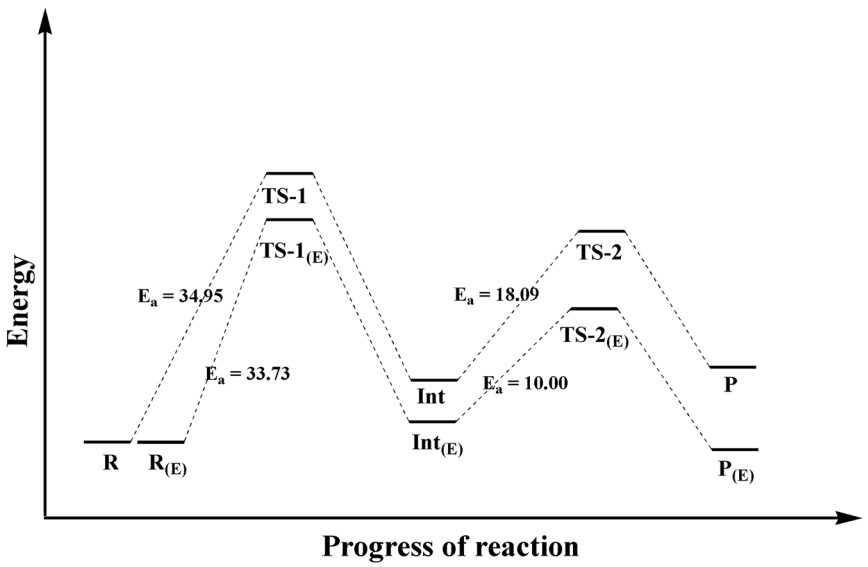

Fig. 3 Potential energy diagram for CO_2 conversion to cyclic carbonate.

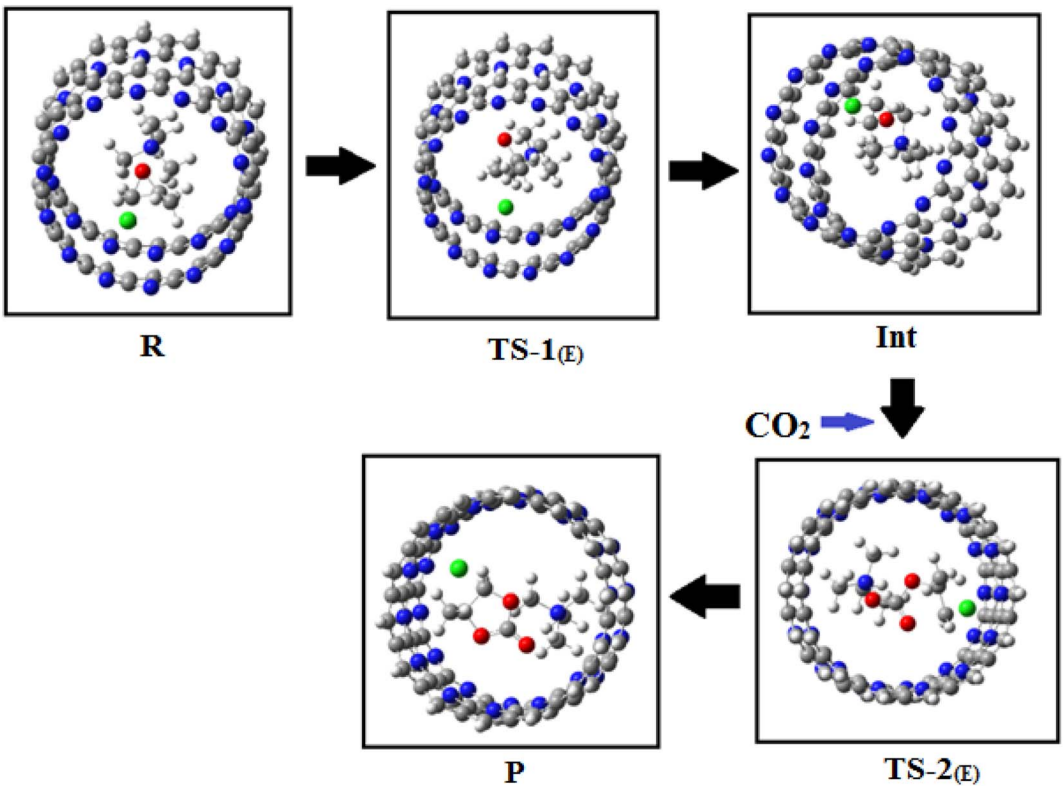

Fig. 4 CO_2 conversion – reaction mechanism with encapsulated ionic liquid (BP-TMACl).

considered. Reactant-2 is not mentioned in Fig. 2. It's the combination of the ring opened PO and CO_2.

For both the steps, the barrier is lower with encapsulated ionic liquid and higher with un-encapsulated ionic liquid. Fig. 3 presents the potential energy profile for comparison of energy barriers with TMACl and BP-TMACl. This points towards the more thermodynamic feasibility of CO_2 conversion with BP-TMACl as compared to un-encapsulated ionic liquid (TMACl). The effect of confinement is quite evident in the results of energy barriers calculated for both the steps of the reaction

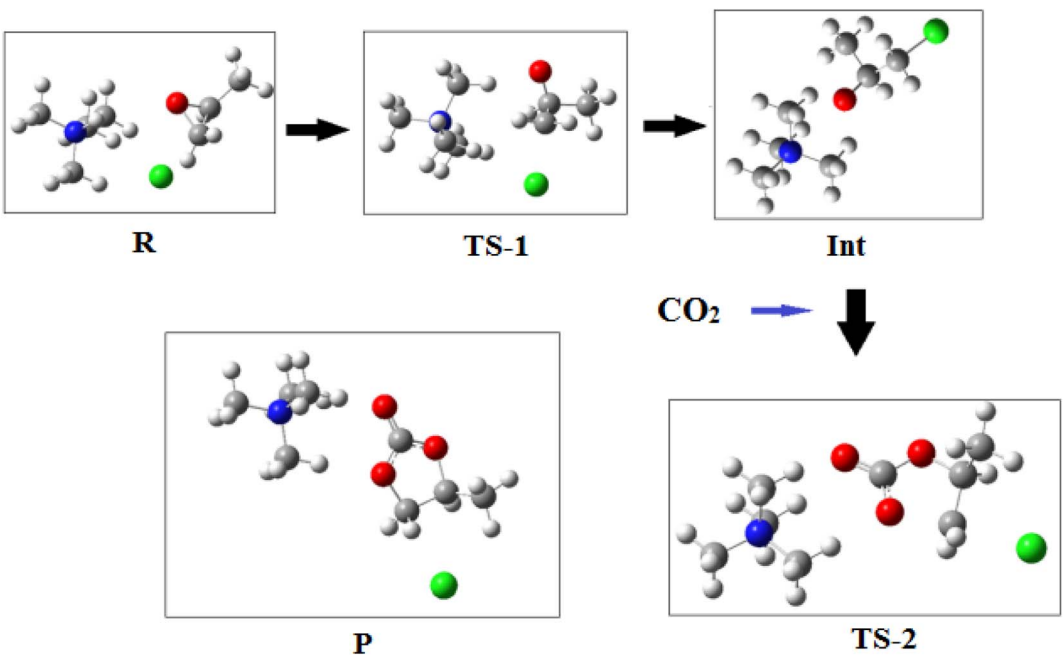

Fig. 5 CO_2 conversion – reaction mechanism with un-encapsulated ionic liquid (TMACl).

(with BP-TMACl). Inside the belts' cavity, the effect of confinement is such that the belts stabilize the reactants and transition state species ultimately lowering the overall energy difference between the complexes (reactants and transition states). Confinement overall lowers the freedom of movement of the reacting species and lowers the energy of transition state specie (specifically) in this way.

Moreover, we observe that for the first step of reaction with both TMACl and BP-TMACl, the energy barriers for the first transition states *i.e.*, TS-1 and TS-$1_{(E)}$, where opening of PO takes place are higher as compared to the second step where CO_2 is utilized in the reaction and is converted to the product. The reason for lower energy barrier in the second step of the reaction is strong nucleophilic nature of oxyanion which attacks the carbon atom of CO_2 easily thus involving the molecule of CO_2 in the formation of propylene carbonate. Although for TS-1, the opening of ring of PO occurs which is the process in which ring strain is released. Yet the barrier for TS-2 is lower. This can be due to the fact that in case of TS-2 there are three oxygen atoms in the structure which develop strong hydrogen bonding interactions with the atoms of the catalyst (ILs). The larger number of electronegative sites which are prone to developing stronger interactions with the atoms of ILs (especially hydrogen atoms of cation) overall bring the TS-2/TS-$2_{(E)}$ to lower energy as evident from their energies (as compared to TS-1/TS-$1_{(E)}$). So, we can say that the TS-2 is more stabilized as compared to TS-1 (in case of both the ILs) due to stronger interactions between components of TS-2 specie and ILs (catalyst) *i.e.*, three electronegative oxygen atoms (with one oxygen completely negatively charged) and one positively charged carbon atom. Moreover, as the step with higher energy barrier controls the overall rate of the reaction therefore step I is the rate limiting step of the reaction for both catalytic systems *i.e.*, both TMACl and BP-TMACl. Additionally, our results are consistent with the previously reported studies on CO_2 conversion with ionic liquids which say that the energy barrier for the CO_2 insertion step is usually small as compared to the ring opening step as no formation or cleavage of bond is involved in this step.[61]

3.3 Reaction energetics (ΔH and ΔG)

Furthermore, the Gibbs free energy change (ΔG) has been calculated (through eqn (2)) for each elementary step of the reaction in order to assess the thermodynamic feasibility of CO_2 conversion reaction with TMACl in encapsulated and unencapsulated forms. The results of ΔG (given in Table 1) show that for the first step of reaction, the ΔG changes from 12.33 kcal mol^{-1} (with TMACl) to 11.08 kcal mol^{-1} (with BP-TMACl). However, the ΔG changes from 10.59 kcal mol^{-1} (with TMACl) to −9.84 kcal mol^{-1} (with BP-TMACl) for second step of the reaction. We can say that the first step of reaction *i.e.*, rate limiting step of overall reaction, is endergonic in nature with both the forms of IL (TMACl and BP-TMACl). However, for second step of the reaction, it's exergonic in nature with BP-TMACl while it's endergonic with TMACl. Hence, overall more thermodynamic feasibility is shown by BP-TMACl as catalyst.

3.4 Electronic characteristics

3.4.1 Frontier molecular orbital (FMO) analysis. According to the HOMO–LUMO gaps (H–L gaps) analyses, the complexes containing reactant and transition state species with

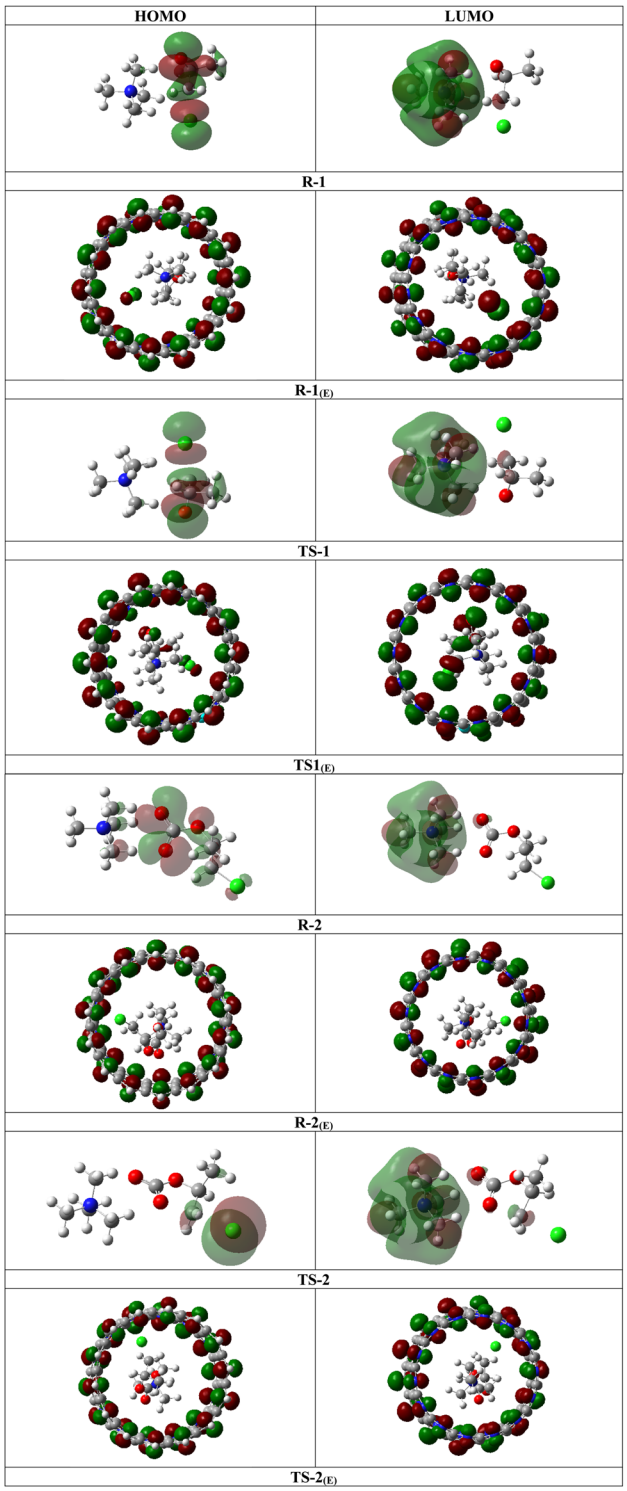

Fig. 6 HOMO and LUMO densities of reactants and transition state species with TMACl and BP-TMACl (the green and red colors represent the positive and negative phases (signs) of the molecular orbital wavefunction, respectively).

encapsulated TMACl (BP-TMACl) show very small values of H–L gaps as compared to the H–L gaps calculated for complexes with un-encapsulated TMACl. In fact, these smaller values of H–L gaps (ranging from 0.26–0.27 eV) match the H–L gap of the belt (bare) showing the effect of belt.

Considering BP as one fragment and TMACl, PO, and CO_2 (reactants) together as a second fragment encapsulated inside BP, we observe that the merging of the energy levels of belt and ionic liquid/reactants (lying inside belt) cannot be seen when reaction takes place inside belt. The reason is difference in energies of HOMO (E_H) and LUMO (E_L) of the fragments (*i.e.*, BP and reactant/transition state) which doesn't allow the merging of energy levels. The reason behind different E_H and E_L values is different nature or composition of the interacting species. One is ionic liquid/reactants with a cation, an anion, propylene oxide and CO_2 while the other one is assembled belt (BP) with much delocalized electrons. Belt has 14 pyridine units fused together which leads to significant delocalization. The effect is further pronounced when the second belt is assembled with the first one. In BP, the HOMO and LUMO both lie on the atoms of belt (Fig. 6). However, in case of ionic liquid (TMACl)/reactants, HOMO lies over chloride (anion part) and oxygen atoms of PO while LUMO lies mainly over cationic part of the ionic liquid. The structural differences between BP and ionic liquid/reactants lead to quite different HOMO and LUMO energy values which ultimately affect the merging of their orbitals when TMACl-reactants are placed inside BP or encapsulated in BP. Hence, even after encapsulation in BP, the HOMO and LUMO orbitals of BP remain unchanged *i.e.*, lying over atoms of belt (Fig. 6).

3.5 Non-covalent interactions (NCI) analysis

In order to analyze the nature of interactions between the fragments of complexes, NCI analysis is performed. These interactions have influence on the energy barriers of the reaction. NCI analysis gives visual illustration of interactions through 3D structures and 2D graphs of the complexes under study. The analysis works through a color scheme where each color in the structure and graph depicts a specific type of interaction. In graphs as well as 3D structures, greenish-brown color represents non-covalent interactions (London dispersion forces and dipole–dipole forces), while the hydrogen bonding is illustrated by blue color. Moreover, red color is the depiction of repulsive forces. Additionally, the graph is generated between $\lambda_2(\rho)$ and reduced density gradient.

The main purpose of NCI analysis in the current study is to understand the reason behind the differences in energy barriers calculated for reaction with bare TMACl and BP-TMACl in CO_2 conversion process. The results of NCI analysis are given in Fig. 7.

Discussing these energy barriers one by one for each step of a reaction, we see that the energy barrier for first transition state (TS-1) reduces from 34.95 kcal mol^{-1} (with TMACl) to 33.73 kcal mol^{-1} (with BP-TMACl) which shows that the energy difference between the reactant and transition state species is reduced in case of BP-TMACl as compared to TMACl. The

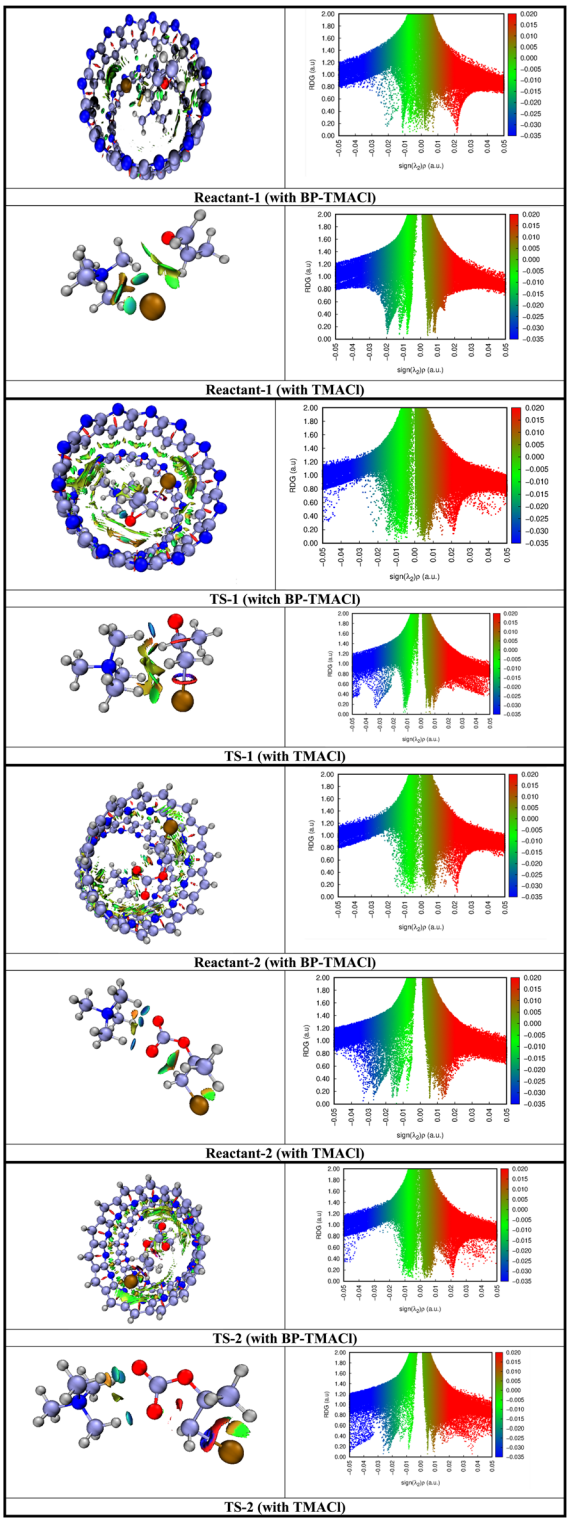

Fig. 7 Results of NCI analysis computed at WB97XD/6-31G(d,p).

results of NCI analysis show that in case of reaction with TMACl, the TS-1 specie shows strong electrostatic interactions (blue colored patches and blue spikes) developed between negatively charged oxygen of oxyanion part and hydrogen atoms of the cation. Moreover, the electrostatic interactions can also be seen between the carbon atom of the oxyanion (positively charged)

and the chloride of TMACl. While, the rest of the atoms show London dispersion forces with the TMACl (greenish brown patches). The nature of these interactions can be confirmed through the graph generated for TS-1 where the blue spikes can be seen in the range of −0.03 to −0.05 au and greenish-brown spikes are present in the range of 0.01 to −0.01 au So, overall quite stronger interactions are observed between the fragments of TS-1 which may result in stabilization of overall specie. The stabilized TS-1 results in a barrier of 34.95 kcal mol^{-1} between R-1 and TS-1. The stabilization of TS-1 is because of the fact that it contains PO (ring opened) containing oxygen and carbon atoms bearing negative and positive charges respectively which are able to develop electrostatic interactions through charged parts and London dispersion forces through the rest of the parts *i.e.*, uncharged.

While, the corresponding reactant (R-1) containing neutral specie in the form of PO with the ring of PO closed shows London dispersion forces developed between PO and TMACl. In the graph generated for R-1, the blue spikes are present but these are the electrostatic interactions between the cation and anion of TMACl (confirmed through the blue patches present in 3D figure). Overall, the interactions are London dispersion forces between PO and TMACl ranging from 0.01 to −0.02 au.

Discussing these interactions for TS-$1_{(E)}$ and $R_{(E)}$ *i.e.*, when reaction takes place in the presence of BP-TMACl, we see that the interactions between the fragments of TS-$1_{(E)}$ and $R_{(E)}$ species are not that different from each other as observed in case of the bare TMACl. Overall, the whole TMACl–PO complex inside the belts' cavity in case of both $R_{(E)}$ and TS-$1_{(E)}$ is stabilized. Both the complexes, due to similar type and strength of interactions inside the belt possess energy closer to one another. However, TS-$1_{(E)}$ possesses slightly stronger interactions *i.e.*, the electrostatic interactions, present between chloride and PO inside the belts (blue spike at −0.05 au) as compared to $R_{(E)}$. These interactions result in bringing TS-$1_{(E)}$ complex even closer in energy to the $R_{(E)}$. These interactions are observed at the chloride part while rest of the complex shows London dispersion forces (in TS-$1_{(E)}$). The corresponding $R_{(E)}$ specie shows only London dispersions forces between the fragments. Overall, the major portion shows London dispersion forces between the fragments in both $R_{(E)}$ and TS-$1_{(E)}$ (lying in the range of 0.01 to −0.02 au in both), hence almost similar kind of interactions result in lower difference in energy between TS-$1_{(E)}$ and $R_{(E)}$. As a result, with BP-TMACl, the energy barrier is calculated to be 33.73 kcal mol^{-1} which is comparatively low than with TMACl. We can see the effect of belts on the barrier in case of BP-TMACl, the atoms of belts stabilize the encapsulated atoms and hence the effect is reflected in reduction in the energy barrier.

Discussing the energy barriers for TS-2 with TMACl, both the TS-2 and R-2 species develop strong interactions between fragments (PO–CO_2 and TMACl). The results of NCI analysis show that both electrostatic interactions and London dispersion forces are present between fragments. The reason behind almost similar kind of interactions is the structural similarity between R-2 and TS-2. Overall, the type of interactions is same as can be observed through similar blue and greenish-brown spikes in the graphs of both species. However, relatively stronger electrostatic interactions (up to −0.05 au) and London dispersion forces (up to −0.03 au) are present in case of TS-2 which results in more stabilization of TS-2 specie. On the other hand, for R-2, values extend up to −0.035 au for electrostatic interactions and up to −0.02 au for London dispersion forces. Hence, for TS-2 the energy barrier is calculated to be 18.09 kcal mol^{-1} which is very low as compared to the barrier for TS-1. Moreover, in case when this second step proceeds with BP-TMACl, the energy barrier drops to 10 kcal mol^{-1}. In this case, the NCI analysis shows that TS-$2_{(E)}$ and R-$2_{(E)}$ species show very similar kind of interactions between the fragments which results in less difference of energies between both the species. Again the effect of confinement can be seen in this step of the reaction. With TMACl, the barrier is already not that high and after the involvement of belts in case of BP-TMACl, the energy barrier drops to even lower value.

Although the energy barriers are not very high with bare TMACl yet encapsulated TMACl reduces them further thus increasing the thermodynamic feasibility of the reaction. The reason behind reduction in barriers with BP-TMACl seems to be the involvement of atoms of belt. Belt overall stabilizes TMACl and other reactants (PO and CO_2) inside the cavity in such a way that overall when reactant moves to transition state overall the difference in energies of the whole complexes (reactants) is small with transition states (both TS-$1_{(E)}$ and TS-$2_{(E)}$) thus resulting in smaller energy barriers. Moreover, NCI results support the results of the energy barriers calculated for reaction with TMACl and BP-TMACl.

3.6 QTAIM analysis

As per the NCI analysis, the nature and strength of interactions affect the energy barriers involved in CO_2 conversion reaction. In order to have further insight into these interactions' strength and validation of their nature, quantum theory of atoms in molecules (QTAIM) analysis[57,65] is considered. The detailed interaction study will help in understanding the energy barriers involved in CO_2 conversion process.

In QTAIM analysis, a different approach is followed for studying interactions between fragments.[53,66] In this method, the most probable interaction sites between reactants/transition states and the ionic liquid (both in encapsulated form and un-encapsulated form) have been analyzed.[66] These areas are known as bond critical points (BCPs). After spotting BCPs, some of the parameters are calculated for these BCPs which help in evaluation of the type of interactions at these BCPs. The values calculated for these parameters (for each BCP) help in understanding the nature of intermolecular interactions which exist between the interacting fragments. Table 2 contains the values calculated for all these parameters for each BCP while Fig. 8 shows the BCPs in the complexes of reactants and transition state species.

Electron density (ρ) calculated for BCPs helps in estimating the strength of interactions. Generally, the values of electron density are positive and most probably greater than 0.1 au for the BCPs showing covalent bonding between the atoms. While,

Table 2 The results of QTAIM study

Complexes	BP-ILs	ρ (au)	$\nabla^2\rho$ (au)	$V_{(r)}$ (au)	$G_{(r)}$ (au)	$-V/G$	E_{int} (kcal mol^{-1})
R-1$_{(E)}$	H149···Cl168	0.007	0.019	−0.003	0.004	0.75	−0.94
	H150··· N67	0.005	0.015	−0.002	0.003	0.67	−0.63
	O144···C154	0.011	0.044	−0.008	0.009	0.89	−2.51
	H147···N58	0.007	0.021	−0.003	0.004	0.75	−0.94
	H150···N167	0.005	0.015	−0.002	0.003	0.67	−0.63
	O144···N68	0.005	0.017	−0.003	0.004	0.75	−0.94
	H145···N68	0.004	0.015	−0.002	0.003	0.67	−0.63
	H148···N57	0.001	0.004	−0.0005	0.0007	0.71	−0.15
TS1$_{(E)}$	O144···C8	0.038	0.011	−0.008	0.009	0.89	−2.51
	C143··· Cl168	0.0001	0.0009	−0.0001	0.0001	1.00	−0.03
	O144···H162	0.013	0.035	−0.009	0.009	1.00	−2.83
	H148···H165	0.006	0.020	−0.003	0.004	1.00	−0.94
	H147···N69	0.014	0.004	−0.002	0.003	0.67	−0.63
	H147···N58	0.014	0.004	−0.002	0.003	0.67	−0.63
	H150···C23	0.009	0.003	−0.001	0.002	0.67	−0.31
R-2$_{(E)}$	C74···O170	0.008	0.027	−0.005	0.006	0.83	−1.57
	C72···O170	0.006	0.024	−0.004	0.005	0.80	−1.26
	H163··· O170	0.017	0.047	−0.013	0.012	1.08	−4.08
	H167···O170	0.017	0.046	−0.012	0.012	1.00	−3.77
	H158··· O169	0.021	0.053	−0.015	0.014	1.07	−4.71
TS2$_{(E)}$	C97···H149	0.004	0.012	−0.002	0.002	1.00	−0.63
	Cl171···C143	0.058	0.069	−0.039	0.028	1.39	−12.24
	H121···H149	0.004	0.012	−0.002	0.002	1.00	−0.63
	C76···O144	0.003	0.011	−0.002	0.002	1.00	−0.63
	H167···O170	0.014	0.040	−0.009	0.009	1.00	−2.82
	C74···O170	0.006	0.022	−0.004	0.005	0.80	−1.26
R-1	Cl28···H8	0.007	0.022	−0.003	0.004	0.75	−0.94
	Cl28···H9	0.007	0.021	−0.003	0.004	0.75	−0.94
	H22···O4	0.011	0.040	−0.007	0.009	0.78	−2.19
TS-1	O4···H22	0.032	0.072	−0.023	0.021	1.09	−7.22
	H8···H25	0.009	0.032	−0.005	0.006	0.83	−1.57
	H9···H19	0.011	0.041	−0.007	0.009	0.78	−2.19
R-2	O30···H27	0.026	0.070	−0.019	0.019	1.00	−5.96
	O30···H23	0.026	0.070	−0.020	0.019	1.05	−6.28
	O29···H18	0.032	0.082	−0.024	0.022	1.09	−7.53
TS-2	Cl31···C3	0.046	0.076	−0.030	0.025	1.20	−9.41
	O29···H18	0.024	0.064	−0.018	0.017	1.06	−5.65
	O30···H27	0.022	0.061	−0.017	0.016	1.06	−5.33
	O30···H23	0.022	0.062	−0.017	0.016	1.06	−5.33

the values are negative and less than 0.1 au for BCPs showing non-covalent interactions between the atoms. Another important parameters *i.e.*, Laplacian of electron density ($\nabla^2\rho$) also helps in analyzing the nature of interactions. Generally, when the values of $\nabla^2\rho$ are positive, it shows non-covalent interactions between the interacting species while negative values of $\nabla^2\rho$ show covalent bonding. Yet another parameter, $-V/G$, further helps in understanding the interactions involved in encapsulation. For weak interactions, value of $-V/G$ is below 1, for interactions of moderate strength $-V/G$ ranges from 1 to 2 and for strong interactions $-V/G$ is more than 2.[67,68] Moreover, interaction energies of individual bonds (E_{int}) can also be calculated through the variables attained through QTAIM study. The E_{int} acquired through QTAIM study is said to be calculated through Espinosa approach where,

$$E_{int}\ (\text{au}) = \tfrac{1}{2}V_{(r)}$$

For the reaction in the presence of TMACl, as per NCI analysis, the type of interactions vary between TS-1 and R-1. In case of TS-1 stronger interactions are present while in the corresponding reactant, R-1, weaker interactions are present. The same results are shown by QTAIM analysis where for TS-1, the interactions range from London dispersion forces to hydrogen bonding. With total three BCPS *i.e.*, O4···H22, H8···H25, and H9···H19, the interactions are strong hydrogen bonding (at O4···H22) while there are London dispersion forces at the other two BCPs (H8···H25, and H9···H19). In case of R-1, relatively weaker interactions are observed through QTAIM analysis. With the three BCPs *i.e.*, Cl28···H8, Cl28···H9, and H22···O4, the interactions lie in the range of London dispersion forces. At all of these BCPs, the interactions are London dispersion forces as revealed through the values of parameters given in Table 2. The reason behind strong interactions between fragments of TS-1 specie is the opened ring of PO with charged atoms showing stronger interactions with the TMACl as compared to the R-1 specie with neutral reactant (PO) having the ring closed. After

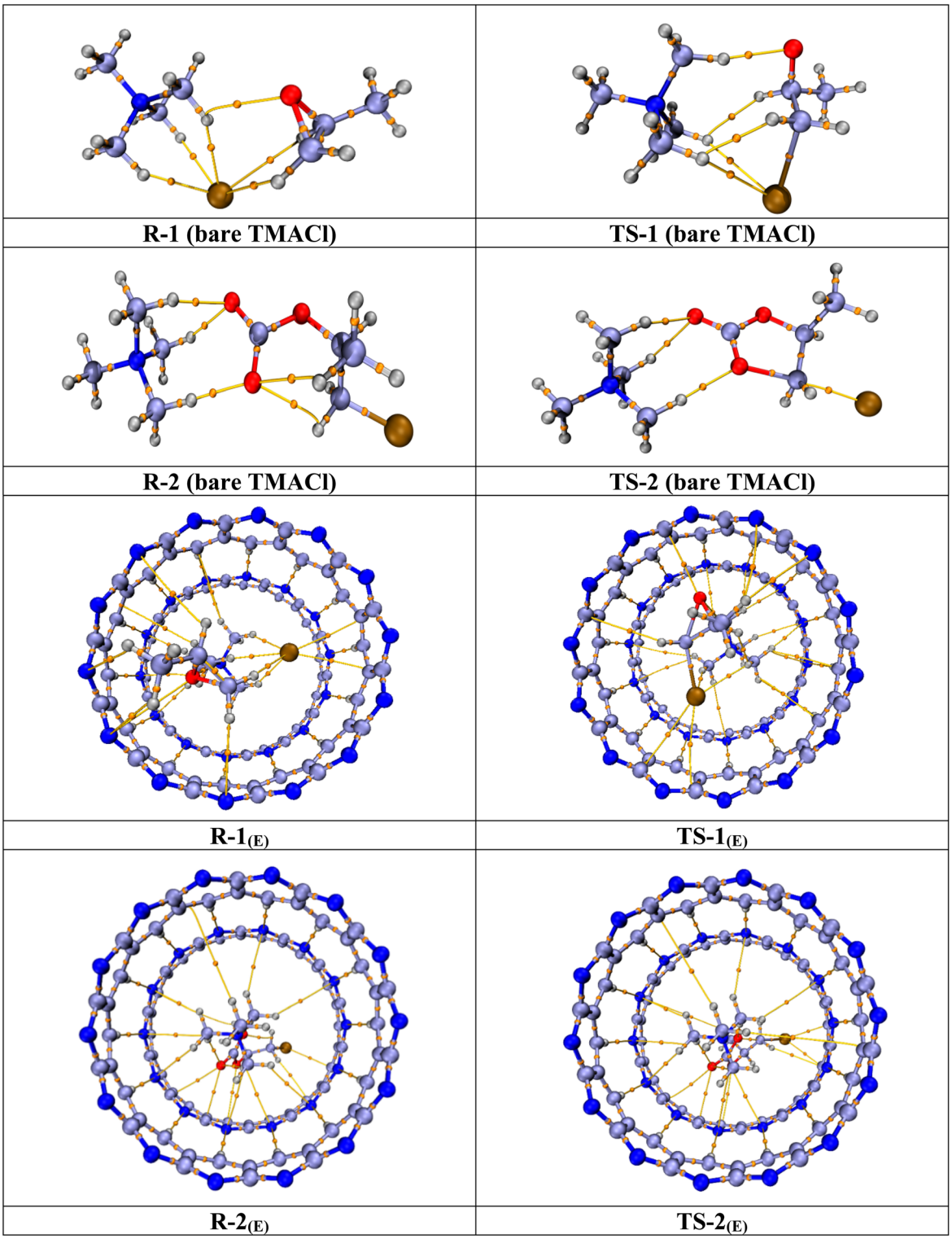

Fig. 8 BCPs obtained through QTAIM analysis.

analyzing interactions, we can say that difference of interactions between fragments (with TS-1 stabilized in the presence of TMACl) leads to an energy barrier of 34.95 kcal mol^{-1}.

For BP-TMACl, the noted BCPs are analyzed in detail through various parameters. We see that, the BCPs in this case are between the atoms of reactants/transition states and atoms of encapsulated ionic liquid (including both the atoms of belt and ionic liquid). The values of parameters for both R-$1_{(E)}$ and TS-$1_{(E)}$ lie in the range of non-covalent interactions. The values of electron density are positive and less than 0.1 au for these two

species. The values of Laplacian of electron density are positive pointing toward involvement of non-covalent interactions. $-V/G$ ranges between 0.67 to 1 in these two species and E_{int} lies in the range of −0.03 to −2.83 kcal mol^{-1} thus confirming non-covalent interactions involved. But, slightly greater values in case of TS1$_{(E)}$ point towards stronger interactions between reactants and surrounding atoms in TS-1$_{(E)}$ complex. Overall, more stabilizing effect of the atoms of BP-TMACl on TS1$_{(E)}$ brings the TS1$_{(E)}$ slightly closer in energy to R-1$_{(E)}$ which ultimately affects the energy barrier for TS1$_{(E)}$. Comparing reactant (R-1/R-1$_{(E)}$) and transition state (TS-1/TS-1$_{(E)}$) species, it can be noticed that the difference in energies between R-1 and TS1 (in case of un-encapsulated TMACl) is more than the difference in energies of R-1$_{(E)}$ and TS1$_{(E)}$. The reason is, inside the belt, the reactants are stabilized such that almost similar kind of interactions brings the R-1$_{(E)}$ and TS1$_{(E)}$ species closer in energies. The slightly higher values of the parameters studied through QTAIM analysis (Table 1) for BCPs of TS1$_{(E)}$ than for R-1$_{(E)}$ shows that TS-1$_{(E)}$ is stabilized more with BP-TMACl, hence overall reducing the barrier for this step of reaction. The effect of belt is such that it overall stabilizes both the reactant and transition state to almost same extent with somewhat stronger interactions for transition state that brings it even closer in energy to reactant. The structure of TS1$_{(E)}$ with ring of propylene oxide opened having oxygen and carbon atoms bearing negative and positive charges respectively and comparatively more polarity in the structure (inside the belts cavity) is more prone to developing interactions with the surrounding atoms as compared to the R-1$_{(E)}$ with comparatively neutral structure or less polar structure. So, overall barrier is controlled by the whole environment of the reactants. TMACl along with the atoms of belt bring R-1$_{(E)}$ and TS1$_{(E)}$ complexes closer in energy which affects the energy barrier involved in this step.

For the TS-2/TS-2$_{(E)}$, with both TMACl and BP-TMACl, the energy barrier for the second transition state in the second step of the reaction is lowered as compared to the first transition state. Moreover, the energy barrier for second transition state is also lowered when reaction is performed with BP-TMACl as compared to reaction with TMACl. In this case, the lowering of energy barrier is from 18.09 kcal mol^{-1} (with TMACl) to 10.00 kcal mol^{-1} (with BP-TMACl). The reason behind lower barrier with BP-TMACl is the same as that discussed in case of the first step of this reaction *i.e.*, the stabilizing effect of the belts. The belts overall bring the reactant and transition state species closer in energy. In this respect, the results of QTAIM analysis show that for certain BCPs of TS-2$_{(E)}$, the values of all the parameters are quite high. For BCP between Cl171⋯C143, the value of E_{int} is equal to −12.24 kcal mol^{-1} showing that attractive forces are very strong hydrogen bonding interactions. $-V/G$ is also equal to 1.39 showing comparatively strong interactions at this BCP. Such strong interactions stabilize the TS-2$_{(E)}$ specie and lower the energy of TS-2$_{(E)}$ which ultimately brings the TS-2$_{(E)}$ and R-2$_{(E)}$ closer in energy and energy barrier is calculated to be quite low.

Moreover, the results of QTAIM analysis support the results of NCI analysis and results of energy barriers calculated for reaction with TMACl and BP-TMACl.

4 Conclusions

Owing to the efficient CO_2 capturing abilities of ENILs as compared to un-encapsulated ILs, we have considered an encapsulated ionic liquid *i.e.*, belt[14]pyridine encapsulated tetramethylammonium chloride (BP-TMACl), in the current study for the purpose of conversion of CO_2 to cyclic carbonate. For comparison, the conversion of CO_2 with both the encapsulated and un-encapsulated forms of TMACl is studied. The results show that encapsulation of ILs enhances their catalytic performance for CO_2 conversion and the energy barriers for both the steps of the reaction are reduced in the presence of (BP-TMACl) as compared with un-encapsulated IL (TMACl). The barriers decrease from 34.95 to 33.73 kcal mol^{-1} (first step) and 18.09 kcal mol^{-1} to 10.00 kcal mol^{-1} (second step), showing improved reactivity of TMACl after encapsulation. Moreover, further analysis supports the results of the energy barriers. According to NCI and QTAIM analysis, the interactions in case of reaction with BP-TMACl are such that belt overall stabilizes the reactant and transition state species inside the cavity thus resulting into reduction in energy barriers. Hence, overall increasing the thermodynamic feasibility of the reaction. Moreover, the values of energy of the reaction (ΔG) also show an overall exergonic nature of the reaction with encapsulated TMACl (BP-TMACl) showing more thermodynamic feasibility of CO_2 conversion with encapsulated TMACl. So, as CO_2 conversion using ILs is well-established but we have proposed a novel approach involving ENIL – an untested method that offers a more efficient way for intensified process of CO_2 utilization.

Conflicts of interest

There are no conflicts of interest to declare.

Data availability

The data supporting this article have been included as part of the supplementary information (SI). Supplementary information: cartesian coordinates of the reactants, transition states & intermediates. The NCI analysis results computed at B3LYP/6-31G(d,p). See DOI: https://doi.org/10.1039/d5ra06369h.

References

1 T. R. Anderson, E. Hawkins and P. D. Jones, CO2, the greenhouse effect and global warming: from the pioneering work of Arrhenius and Callendar to today's Earth System Models, *Endeavour*, 2016, **40**(3), 178–187.
2 P. Campitelli, *et al.*, CO2 Capture and Conversion to C1 Chemicals with Mixed-Metal Copper/Nickel Bis (amino) bipyrazolate Metal–Organic Frameworks, *ACS Appl. Energy Mater.*, 2023, **6**(18), 9231–9242.
3 D. Jansen, *et al.*, Pre-combustion CO2 capture, *Int. J. Greenh. Gas Control*, 2015, **40**, 167–187.
4 E. I. Koytsoumpa, C. Bergins and E. Kakaras, The CO2 economy: Review of CO2 capture and reuse technologies, *J. Supercrit. Fluids*, 2018, **132**, 3–16.

5 T. Uchida, *et al.*, Oxyfuel combustion as CO2 capture technology advancing for practical use-Callide oxyfuel project, *Energy Procedia*, 2013, **37**, 1471–1479.
6 X. Liu, *et al.*, Low-carbon economic dispatch of integrated electricity-gas energy system considering carbon capture, utilization and storage, *IEEE Access*, 2023, **11**, 25077–25089.
7 T. Sakakura and K. Kohno, The synthesis of organic carbonates from carbon dioxide, *Chem. Commun.*, 2009, (11), 1312–1330.
8 H. Büttner, *et al.*, Recent developments in the synthesis of cyclic carbonates from epoxides and CO_2, in *Chemical Transformations of Carbon Dioxide*, 2018, pp. 89–144.
9 M. H. Beyzavi, *et al.*, Metal–organic framework-based catalysts: chemical fixation of CO2 with epoxides leading to cyclic organic carbonates, *Front. Energy Res.*, 2015, **2**, 63.
10 M. Cokoja, *et al.*, Synthesis of cyclic carbonates from epoxides and carbon dioxide by using organocatalysts, *ChemSusChem*, 2015, **8**(15), 2436–2454.
11 B.-H. Xu, *et al.*, Fixation of CO 2 into cyclic carbonates catalyzed by ionic liquids: a multi-scale approach, *Green Chem.*, 2015, **17**(1), 108–122.
12 F. D. Bobbink and P. J. Dyson, Synthesis of carbonates and related compounds incorporating CO2 using ionic liquid-type catalysts: State-of-the-art and beyond, *J. Catal.*, 2016, **343**, 52–61.
13 J. Peng and Y. Deng, Cycloaddition of carbon dioxide to propylene oxide catalyzed by ionic liquids, *New J. Chem.*, 2001, **25**(4), 639–641.
14 C. Moya, *et al.*, CO2 conversion to cyclic carbonates catalyzed by ionic liquids with aprotic heterocyclic anions: DFT calculations and operando FTIR analysis, *J. CO2 Util.*, 2018, **28**, 66–72.
15 Q. He, *et al.*, Synthesis of cyclic carbonates from CO 2 and epoxides using ionic liquids and related catalysts including choline chloride–metal halide mixtures, *Catal. Sci. Technol.*, 2014, **4**(6), 1513–1528.
16 F. Wang, *et al.*, Mechanism and origins of enantioselectivity for [BMIM] Cl ionic liquids and ZnCl2 co-catalyzed coupling reaction of CO2 with epoxides, *J. Mol. Catal. A: Chem.*, 2014, **385**, 133–140.
17 J.-Q. Wang, *et al.*, Efficient fixation of CO 2 into organic carbonates catalyzed by 2-hydroxymethyl-functionalized ionic liquids, *RSC Adv.*, 2014, **4**(5), 2360–2367.
18 D. Kim, *et al.*, Metal-containing ionic liquids as synergistic catalysts for the cycloaddition of CO2: a density functional theory and response surface methodology corroborated study, *ACS Sustain. Chem. Eng.*, 2016, **4**(9), 4591–4600.
19 X. Meng, *et al.*, Temperature-controlled reaction–separation for conversion of CO2 to carbonates with functional ionic liquids catalyst, *ACS Sustain. Chem. Eng.*, 2017, **5**(4), 3081–3086.
20 T. Wang, *et al.*, Benzyl substituted imidazolium ionic liquids as efficient solvent-free catalysts for the cycloaddition of CO2 with epoxides: Experimental and Theoretic study, *J. CO2 Util.*, 2017, **22**, 44–52.
21 M. Liu, *et al.*, Heterogeneous catalytic conversion of CO2 and epoxides to cyclic carbonates over multifunctional tri-s-triazine terminal-linked ionic liquids, *J. Catal.*, 2017, **347**, 138–147.
22 X. Zhang, *et al.*, Immobilized protic ionic liquids: Efficient catalysts for CO2 fixation with epoxides, *J. CO2 Util.*, 2017, **17**, 37–42.
23 G. Kaur, H. Kumar and M. Singla, Diverse applications of ionic liquids: A comprehensive review, *J. Mol. Liq.*, 2022, **351**, 118556.
24 A. J. Greer, J. Jacquemin and C. Hardacre, Industrial applications of ionic liquids, *Molecules*, 2020, **25**(21), 5207.
25 K. S. Egorova, E. G. Gordeev and V. P. Ananikov, Biological activity of ionic liquids and their application in pharmaceutics and medicine, *Chem. Rev.*, 2017, **117**(10), 7132–7189.
26 T. Zhou, *et al.*, Energy applications of ionic liquids: recent developments and future prospects, *Chem. Rev.*, 2023, **123**(21), 12170–12253.
27 M. Ahrenberg, *et al.*, Vapor pressure of ionic liquids at low temperatures from AC-chip-calorimetry, *Phys. Chem. Chem. Phys.*, 2016, **18**(31), 21381–21390.
28 C. Maton, N. De Vos and C. V. Stevens, Ionic liquid thermal stabilities: decomposition mechanisms and analysis tools, *Chem. Soc. Rev.*, 2013, **42**(13), 5963–5977.
29 M. J. Earle and K. R. Seddon, Ionic liquids. Green solvents for the future, *Pure Appl. Chem.*, 2000, **72**(7), 1391–1398.
30 N. V. Plechkova and K. R. Seddon, Applications of ionic liquids in the chemical industry, *Chem. Soc. Rev.*, 2008, **37**(1), 123–150.
31 M. Petkovic, *et al.*, Ionic liquids: a pathway to environmental acceptability, *Chem. Soc. Rev.*, 2011, **40**(3), 1383–1403.
32 J. Kestin, M. Sokolov and W. A. Wakeham, Viscosity of liquid water in the range− 8 C to 150 C, *J. Phys. Chem. Ref. Data*, 1978, **7**(3), 941–948.
33 K. R. Harris, L. A. Woolf and M. Kanakubo, Temperature and pressure dependence of the viscosity of the ionic liquid 1-butyl-3-methylimidazolium hexafluorophosphate, *J. Chem. Eng. Data*, 2005, **50**(5), 1777–1782.
34 M. Han, *et al.*, Efficient confinement of ionic liquids in MIL-100 (Fe) frameworks by the "impregnation-reaction-encapsulation" strategy for biodiesel production, *RSC Adv.*, 2016, **6**(43), 37110–37117.
35 K. Matsumoto and T. Endo, Confinement of ionic liquid by networked polymers based on multifunctional epoxy resins, *Macromolecules*, 2008, **41**(19), 6981–6986.
36 D.-x. Chen, *et al.*, Adsorption of caprolactam from aqueous solution by novel polysulfone microcapsules containing [Bmim][PF6], *Colloids Surf., A*, 2014, **441**, 72–76.
37 Z. Xiang, *et al.*, Preparation of microcapsules containing ionic liquids with a new solvent extraction system, *React. Funct. Polym.*, 2008, **68**(8), 1260–1265.
38 H. Gao, *et al.*, Immobilization of ionic liquid [BMIM][PF6] by spraying suspension dispersion method, *Ind. Eng. Chem. Res.*, 2008, **47**(13), 4414–4417.
39 D. Brevet, *et al.*, Self-encapsulation of a drug-containing ionic liquid into mesoporous silica monoliths or nanoparticles by a sol–gel process, *RSC Adv.*, 2016, **6**(86), 82916–82923.

40 K. Pohako-Esko, *et al.*, Chitosan containing supported ionic liquid phase materials for CO2 absorption, *Ind. Eng. Chem. Res.*, 2016, **55**(25), 7052–7059.
41 E. Weiss and R. Abu-Reziq, Ionic liquid-based polymeric microreactors and their applicability, *J. Mater. Sci.*, 2017, **52**, 10637–10647.
42 I. S. Elizarova and P. F. Luckham, Layer-by-layer encapsulated nano-emulsion of ionic liquid loaded with functional material for extraction of Cd2+ ions from aqueous solutions, *J. Colloid Interface Sci.*, 2017, **491**, 286–293.
43 E. Weiss, *et al.*, BMIm-PF6@ SiO2 microcapsules: particulated ionic liquid as a new material for the heterogenization of catalysts, *Chem. Mater.*, 2014, **26**(16), 4781–4787.
44 R. Santiago, *et al.*, From kinetics to equilibrium control in CO2 capture columns using Encapsulated Ionic Liquids (ENILs), *Chem. Eng. J.*, 2018, **348**, 661–668.
45 G. E. Romanos, *et al.*, CO2 capture by novel supported ionic liquid phase systems consisting of silica nanoparticles encapsulating amine-functionalized ionic liquids, *J. Phys. Chem. C*, 2014, **118**(42), 24437–24451.
46 L. Al-Mahbobi, *et al.*, CO2 Capture with Capsules of Ionic Liquid/Amines, *ACS Appl. Eng. Mater.*, 2024, **2**(5), 1298–1305.
47 N. C. Starvaggi, *et al.*, Double emulsion microencapsulation of ionic liquids for carbon capture, *Mater. Horiz.*, 2024, **11**(23), 6057–6063.
48 K. Tahara and Y. Tobe, Molecular loops and belts, *Chem. Rev.*, 2006, **106**(12), 5274–5290.
49 Y. Li, *et al.*, Catalytic activity of a series of synthesized and newly designed pyridinium-based ionic liquids on the fixation of carbon dioxide: a DFT investigation, *Ind. Eng. Chem. Res.*, 2015, **54**(33), 8093–8099.
50 S. K. Shukla, *et al.*, Ionic liquids: Potential materials for carbon dioxide capture and utilization, *Front. Mater.*, 2019, **6**, 42.
51 S. Dorado-Alfaro, *et al.*, Solubility and dissociation of ionic liquids in epoxides and cyclic carbonate by molecular dynamics simulation, *J. Mol. Liq.*, 2025, **426**, 127322.
52 R. Carlsen, J. R. Jenkins and D. H. Ess, Direct dynamics analysis of the cationic Cp*(PMe 3) Ir (CH 3) methane C–H activation mechanism, *Faraday Discuss.*, 2019, **220**, 414–424.
53 A. Ahsan, A. Lakhani and K. Ayub, Encapsulation of ionic liquids in the cavity generated by assembled belt [14] pyridine units–A theoretical study, *Colloids Surf., A*, 2025, **711**, 136369.
54 K. Fukui, Role of frontier orbitals in chemical reactions, *science*, 1982, **218**(4574), 747–754.
55 S. Pan, *et al.*, Selectivity in gas adsorption by molecular cucurbit [6] uril, *J. Phys. Chem. C*, 2016, **120**(26), 13911–13921.
56 T. Lu and F. Chen, Multiwfn: A multifunctional wavefunction analyzer, *J. Comput. Chem.*, 2012, **33**(5), 580–592.
57 R. F. W. Bader, *Theory of Atoms in Molecules*, Oxford University Press, 1995.
58 S. Sarfaraz, *et al.*, DFT investigation of adsorption of nitro-explosives over C2N surface: Highly selective towards trinitro benzene, *J. Mol. Liq.*, 2022, **352**, 118652.
59 Y. S. Al-Faiyz, *et al.*, Efficient Detection of Nerve Agents through Carbon Nitride Quantum Dots: A DFT Approach, *Nanomaterials*, 2023, **13**(2), 251.
60 S. M. Soliman and A. Barakat, Decomposition of intermolecular interactions in the crystal structure of some diacetyl platinum (II) complexes: Combined Hirshfeld, AIM, and NBO analyses, *Molecules*, 2016, **21**(12), 1669.
61 S. Foltran, R. Mereau and T. Tassaing, Theoretical study on the chemical fixation of carbon dioxide with propylene oxide catalyzed by ammonium and guanidinium salts, *Catal. Sci. Technol.*, 2014, **4**(6), 1585–1597.
62 L. Wang, *et al.*, Hydroxyl-functionalized ionic liquid promoted CO2 fixation according to electrostatic attraction and hydrogen bonding interaction, *Ind. Eng. Chem. Res.*, 2014, **53**(20), 8426–8435.
63 J.-Q. Wang, *et al.*, Experimental and theoretical studies on hydrogen bond-promoted fixation of carbon dioxide and epoxides in cyclic carbonates, *Phys. Chem. Chem. Phys.*, 2012, **14**(31), 11021–11026.
64 Z. J. Li, *et al.*, Homogeneous and heterogeneous ionic liquid system: promising "ideal catalysts" for the fixation of CO2 into cyclic carbonates, *ChemCatChem*, 2021, **13**(8), 1848–1866.
65 R. F. Bader, A quantum theory of molecular structure and its applications, *Chem. Rev.*, 1991, **91**(5), 893–928.
66 P. Popelier, On the full topology of the Laplacian of the electron density, *Coord. Chem. Rev.*, 2000, **197**(1), 169–189.
67 A. Kazachenko, *et al.*, Sulfation of diethylaminoethyl-cellulose: QTAIM topological analysis and experimental and DFT studies of the properties, *ACS Omega*, 2021, **6**(35), 22603–22615.
68 U. Gunawan, *et al.*, Theoretical insight and molecular recognition of fluconazole molecularly imprinted polymers: a combined computational and experimental analysis, *RSC Adv.*, 2025, **15**(24), 19158–19175.